



Retrospective Cost Adaptive Control of Unstart in a Model Scramjet Combustor

Ankit Goel,* Karthik Duraisamy,[†] and Dennis S. Bernstein[‡]
University of Michigan, Ann Arbor, Michigan 48109

DOI: 10.2514/1.J055812

A data-enabled adaptive control strategy is developed to regulate the thrust produced by a scramjet engine under normal operating conditions as well as near unstart. Specifically, retrospective cost adaptive control is pursued. Retrospective cost adaptive control is a direct discrete-time adaptive control algorithm that is applicable to stabilization, command following, and disturbance rejection. Retrospective cost adaptive control uses minimal modeling information, past control inputs, and limited measurements to retrospectively optimize the controller coefficients. A two-dimensional computational fluid dynamics model of the Hyshot-II scramjet geometry is used with a heat-release model to represent the dynamics of the combustor. This representation involves coupled nonlinear partial differential equations with $O(10^5)$ degrees of freedom. First, the open-loop dynamic response of the model is studied to estimate essential features of the system. Then, retrospective cost adaptive control is used to maintain the commanded thrust in the presence of a disturbance in the Mach number. Finally, a modified performance variable is defined and is shown to enable retrospective cost adaptive control to suppress unstart.

Nomenclature

G_f	=	retrospective cost adaptive control filter
M	=	inlet Mach number (in the isolator)
M_0	=	constant inlet Mach number
r	=	nondimensionalized thrust command
T_c	=	time step for the controller update
T_s	=	time step for the scramjet update
u_c	=	retrospective cost adaptive controller output
y	=	nondimensionalized thrust
z	=	performance variable
θ	=	dynamic controller coefficients
λ	=	forgetting factor
ϕ	=	fuel–air equivalence ratio
ϕ_0	=	constant fuel–air equivalence ratio

I. Introduction

A SUPERSONIC combustion ramjet (scramjet) engine is an airbreathing propulsion system that has demonstrated potential for high-speed transport, access to space, and payload delivery [1]. A scramjet engine compresses and ignites a supersonic stream of air and generates thrust by expelling high-energy gases through a nozzle. The scramjet engine is mechanically simple because the entire process is achieved with no moving parts.

A complicating factor in the design of a scramjet engine stems from the requirement to maintain internal flow conditions within a narrow range of acceptable limits. Crossing any of these limits, which are dictated by thermodynamics, fluid mechanics, and combustion, may lead to instabilities that can result in catastrophic failure. The ability to control the internal flow conditions and maintain the system thrust in the presence of external disturbances is thus of critical technological value.

Received 31 October 2016; revision received 31 August 2017; accepted for publication 17 November 2017; published online 31 January 2018. Copyright © 2017 by Ankit Goel. Published by the American Institute of Aeronautics and Astronautics, Inc., with permission. All requests for copying and permission to reprint should be submitted to CCC at www.copyright.com; employ the ISSN 0001-1452 (print) or 1533-385X (online) to initiate your request. See also AIAA Rights and Permissions www.aiaa.org/randp.

*Ph.D. Candidate, Department of Aerospace Engineering, 1320 Beal Ave.; ankigoel@umich.edu.

[†]Associate Professor, Department of Aerospace Engineering, 1320 Beal Ave.; kdur@umich.edu.

[‡]Professor, Department of Aerospace Engineering, 1320 Beal Ave.; dsbaero@umich.edu.

The flow inside the scramjet engine, which involves subsonic and supersonic regions, is highly sensitive to the operating conditions. A particularly unforgiving phenomenon is unstart, in which a normal shock is formed in the combustor. Unstart destabilizes the flow, and the shock system travels upstream, leading to a significant loss of thrust and system failure. The need to avoid unstart dictates constraints on the operational envelope of the vehicle.

In [2], the problem of preventing a hypersonic vehicle from unstarting by keeping it in a predefined flight envelope is considered. In [3], a second-order linear, time-invariant transfer function model from the ramp angle to the shock train location is identified. This model was used to tune a proportional–integral–derivative controller, which was applied to the high-order model and used to shift the location of the shock train as a means for preventing unstart. In [4], open-loop simulations are presented to establish unstart limits. In [5], a particle filter was used to estimate the state of a scramjet described by a one-dimensional model, and a full-state-feedback control law was suggested to prevent the scramjet from unstarting. The control altered the cycle length as well as the burst length of the fuel flow based on the predicted future location of the shock front computed using the filtered state. As a precursor to the work in the present paper, retrospective cost adaptive control (RCAC) was applied in [6] to the problem of controlling thrust generated by a one-dimensional scramjet model in the presence of inlet Mach number disturbances.

In the present work, RCAC is applied to command following, disturbance rejection, and unstart prevention in a two-dimensional scramjet model. The control strategy uses the equivalence ratio as the control input, which determines the addition of heat to the vehicle, which in turn affects the internal flow and generated thrust. The dynamics of the scramjet are represented by a two-dimensional computational fluid dynamics model of the centerplane of the Hyshot-II scramjet engine, which was tested in Australia over the past decade [1]. This model is composed of a set of coupled nonlinear partial differential equations that assume inviscid flow along with a simplified heat-release model. These equations are temporally and spatially discretized with $O(10^5)$ degrees of freedom.

Because the control input is the equivalence ratio modulated by the fuel-injection rate, the present paper assumes the availability of a high-speed fuel-injection actuator. In practice, the bandwidth of a physical actuator, such as a pump/valve device, is a critical factor in enabling unstart suppression. The study in the present paper thus provides a step toward understanding the actuation requirements for this application.

RCAC, which was developed in [7–10], is based on minimizing a performance variable that incorporates input–output measurements. For discrete-time linear systems, RCAC requires minimal modeling information, namely, knowledge of the leading sign, relative degree,

and real nonminimum-phase (NMP) zeros. Otherwise, RCAC requires no additional modeling information. A key feature of RCAC is its ability to control systems that have NMP zeros, that is, zeros that lie outside of the open unit disk in the complex plane. NMP zeros are known to present fundamental challenges in feedback control [11].

The present paper considers three control problems, namely, 1) command following, where the goal is to have the thrust output follow a commanded thrust profile consisting of time-dependent steps and ramps; 2) disturbance rejection, where the goal is to maintain the thrust at a specified set point despite the presence of an unknown step disturbance in the operating conditions; and 3) stabilization, where the goal is to prevent the scramjet from unstating. A key difficulty in the second problem arises from the fact that the scramjet dynamics depend nonlinearly on the height of the step disturbance. It should be stressed that RCAC uses measurements of generated thrust and equivalence ratio applied in the past and has no access to additional measurements of internal states of the scramjet. In addition, because RCAC uses the minimal modeling information mentioned previously, it makes no use of detailed modeling information such as the Jacobian of the model. The modeling information required by RCAC is obtained from identification based on simulation of the model. Nonlinear effects are modeled by parameterizing the identified model in terms of Mach number.

The paper is organized as follows. In Sec. II, we present the key details of the numerical model of the scramjet considered in the paper. In Sec. III, relevant qualitative features of the scramjet are investigated. In Sec. IV, the details of the RCAC algorithm are presented. In Sec. V, we present numerical examples of typical control objectives and use a modified performance variable to prevent the scramjet from unstating. Finally, in Sec. VI, we conclude and discuss future work.

II. Scramjet Model

We use an idealized version of the Hyshot-II scramjet geometry [1,12,13]. The midplane of the isolator, the combustor, and the nozzle section of the geometry of the vehicle are shown in Fig. 1 [13]. Note that the lengths shown are in millimeters, and the simulation domain, which starts at $x = 0.35$ m approximately, is highlighted in yellow. The inflow to the isolator corresponds to the flow after it has been deflected by two shocks from the forebody and cowl in the real vehicle. The flow is assumed to be governed by the two-dimensional Euler equations:

$$\frac{\partial}{\partial t} \begin{bmatrix} \rho \\ \rho u \\ \rho v \\ e \end{bmatrix} + \frac{\partial}{\partial x} \begin{bmatrix} \rho u \\ \rho u^2 + p \\ \rho uv \\ u(e + p) \end{bmatrix} + \frac{\partial}{\partial y} \begin{bmatrix} \rho v \\ \rho uv \\ \rho v^2 + p \\ v(e + p) \end{bmatrix} = \begin{bmatrix} 0 \\ 0 \\ 0 \\ \dot{Q} \end{bmatrix} \quad (1)$$

where ρ is the fluid density; u and v are longitudinal and lateral velocity components, respectively; and p is the pressure. The total energy e per unit volume can be written in terms of the velocity and pressure as

$$e = \frac{p}{\gamma - 1} + \frac{1}{2} \rho u^2 \quad (2)$$

where γ is the ratio of specific heats. These equations have a hyperbolic character in time, and the flow variables include

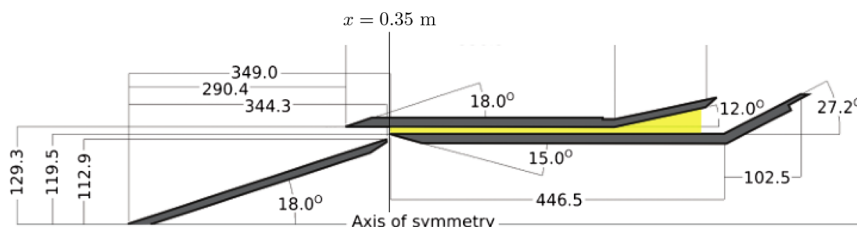


Fig. 1 Geometry of the Hyshot-II scramjet engine [13].

Table 1 Summary of parameters used in the heat-release model [Eqs. (3) and (4)]

Symbol	Definition	Nominal value
f_{st}	Stoichiometric fuel/air ratio	0.028
H_f	Fuel heating value (H_2)	120 MJ/Kg
x_c	Combustion ignition position	0.408 m
L_c	Combustor length	0.368 m
K_c	Fraction of completed combustion	0.95
D_c	Shape parameter	0.75
C_c	Shape parameter	$-\log(1 - K_c)^{1/D_c}$

discontinuous profile changes in space and time because of the presence of shock waves.

The simplified heat-release model given in [14] is used to represent the combustion process. The cumulative heat release, which is represented by the source term \dot{Q} in the energy Eq. (1), is modeled by

$$\dot{Q} = \phi f_{st} H_f \dot{m}_{air} \eta(x/L_c) \quad (3)$$

$$\eta(x/L_c) = 1 - e^{-(C_c(x-x_c)/L_c)^{D_c}} \quad (4)$$

where $x_c < x < x_c + L_c$, ϕ is the fuel–air equivalence ratio, and η is the heat-release distribution function. The parameters in Eqs. (3) and (4) are given in Table 1. All numerical computations are performed using the unstructured mesh compressible flow solver Joe [13,15,16]. Because of the inviscid flow assumption and the simplified heat-release model, the simulation model does not capture shock/boundary-layer interactions and details of turbulent combustion.

Figure 2 shows illustrative contours of the density gradients in the solution domain. Note that the combustion starts at $x = x_c$, and the expanding section is the nozzle. Figure 3 compares the pressure on the lower wall of the engine with experimental measurements reported in [12]. The red curve denotes the simulated normalized static pressure, and the blue dots with error bars are the measurements. Both of these plots correspond to a steady operating state at the equivalence ratio $\phi = 0.35$. In [12,17], the model [Eqs. (1) and (3)] was confirmed to predict unstart at roughly the same equivalence ratio $\phi \approx 0.39$ as in ground experiments.

The heat release is controlled by varying the fuel-injection rate and thus the equivalence ratio. In the present paper, the fuel-injection rate thus serves as the control input. To do this, a high-bandwidth fuel-injection actuator is assumed, and the dynamics of the actuator (such as a pump/valve device) are not considered. This assumption facilitates fast reaction to unstart. This point is further discussed in Sec. VI. Finally, the thrust generated is computed by integrating the pressure along the flow path. The computed thrust is normalized and nondimensionalized by the freestream dynamic pressure and unit area.

III. Analysis of the Scramjet Dynamics

In this section, we simulate the scramjet without feedback control to characterize its dynamics. First, the step response is used to determine the operating envelope of the scramjet. Next, the impulse response is used to extract the modeling information required by RCAC. Note that the scramjet is a single-input/single-output system with equivalence ratio ϕ as the input and the generated thrust as the output y .

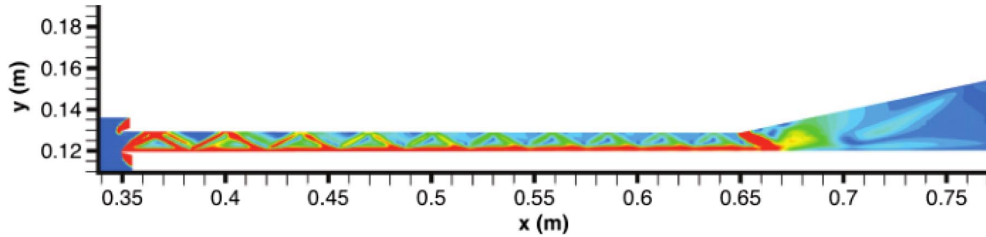


Fig. 2 Contours of density gradient magnitudes over the simulation domain shown in Fig. 1.

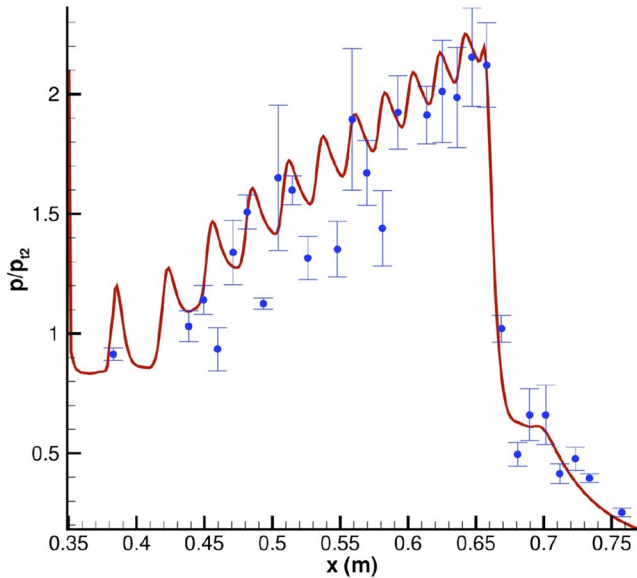


Fig. 3 Normalized pressure on the lower wall of the simulated HyShot-II isolator/combustor.

A. Step Response

One of the major challenges in scramjet operation is unstart. When sufficient heat is released in the combustor, the flow can thermally choke, which leads to a normal shock traveling upstream, eventually establishing subsonic flow in the combustor and the isolator region. This phenomenon can be structurally and thermally fatal to the engine operation. It is also well known that the engine can unstart due to inlet flow perturbations [18], structural deformation [19], or excessive heat addition. Because of the possibility of unstart, there is an upper bound on the steady-state thrust that can be generated by the scramjet at a given operating condition. The maximum steady-state thrust that can be generated by the scramjet at a constant inlet Mach number M_0 is called the critical thrust at M_0 , and the constant equivalence ratio ϕ_0 that produces critical thrust is called the critical equivalence ratio at M_0 .

The scramjet dynamics described by Eq. (1) may or may not have an equilibrium state for a constant inlet Mach number M_0 and a constant equivalence ratio ϕ_0 . If, at a given constant inlet Mach number M_0 and a constant equivalence ratio ϕ_0 , the scramjet reaches a steady state, then we say that the scramjet is not unstarting. If, on the other hand, the scramjet state diverges, we say that the scramjet is unstarting.

To illustrate the previous discussion, consider the scalar dynamical model

$$\dot{x} = x^2 + \alpha x + \beta \quad (5)$$

where x , α , β are real numbers. Depending on the values of α and β , equilibria may exist, and if they exist, they may or may not be stable. If an equilibrium exists, we can analyze the linearized model to deduce the stability of the equilibrium point. Because the scramjet model in this work has $O(10^5)$ degrees of freedom, computing an equilibrium point for a given inlet Mach number M_0 and an equivalence ratio ϕ_0 is computationally intractable. Therefore, we

use the step response of the scramjet to determine the critical thrust and critical equivalence ratio at a given operating condition.

To obtain the step response, we simulate the scramjet with the equivalence ratio $\phi(k) = \phi_0$, and the inlet Mach number $M(k) = M_0$ for all $k \geq 1$. The time step T_s used to update the scramjet state is 5×10^{-4} ms. The continuous-time variable t and the discrete-time variable k are related by $t = kT_s$.

Figure 4 shows the open-loop step response of the scramjet at various constant inlet Mach numbers for several values of the constant equivalence ratio ϕ_0 . At each inlet Mach number M_0 , the scramjet flow reaches a steady state for a low equivalence ratio and unstarts at a higher equivalence ratio.

Figure 5 shows the thrust generated by the scramjet at the end of each simulation for various constant inlet Mach numbers and constant equivalence ratios. Each solid dot represents one simulation. The abscissa is the constant equivalence ratio applied to the scramjet, and the ordinate of the point is the thrust generated by the scramjet at the end of the simulation. Note that, for each value of M_0 , the scramjet flow reaches a steady state and generates a constant thrust for ϕ_0 to the left of the corresponding vertical dashed line of the same color. To the right of the vertical dashed line, the scramjet flow is unsteady; in fact, the scramjet is unstarting. Hence, the thrust generated by the scramjet, as denoted by a circle for each inlet Mach number M_0 , is the computed critical thrust at M_0 . Note that the actual critical thrust may be greater than the computed value because only a finite number of cases are simulated. Nevertheless, this technique yields a lower bound for the critical thrust at M_0 .

Figure 6 shows the normalized static pressure along the lower wall of the scramjet at various inlet Mach numbers for the constant inlet Mach number M_0 and the constant equivalence ratio ϕ_0 labeled on the top of the figure, at various times. Note that the static pressure is normalized by the freestream pitot pressure value. The plots in the left column show simulations where the flow reaches steady state. The thrust generated at the end of these simulations is the critical thrust. The plots in the right column show simulations where the scramjet is unstarting, as indicated by the normal shock traveling toward the inlet.

B. Impulse Response

Because linear systems satisfy the principle of superposition, the state of the system and the input do not affect the impulse response. In a nonlinear system, however, the impulse response is sensitive to the state of the system at the time at which the impulse input is imposed. Nonetheless, the impulse response at an equilibrium state for a constant input can provide useful insights into the local behavior of the system. In particular, the goal is to determine whether or not the scramjet model possesses real NMP zeros because these zeros are challenging for adaptive control.

To obtain the impulse response, we simulate the scramjet at a constant Mach number $M(k) \equiv M_0$ with a constant equivalence ratio $\phi(k) \equiv \phi_0$. We denote the steady-state thrust generated as y_0 . Once the scramjet reaches equilibrium, we add ϕ_δ to the equivalence ratio for one time step. Consequently, ϕ_δ serves as an impulse in the equivalence ratio. The flowfield reacts to the impulsive heat addition, and the thrust generated by the scramjet $y(k)$ is perturbed before settling back to y_0 . We define the impulse response δy at the equivalence ratio ϕ_0 and the inlet Mach number M_0 as the sequence $y(k) - y_0$. Figure 7a shows the impulse response δy of the scramjet for an impulse with magnitude $\phi_\delta = 0.05$ at $\phi_0 \in \{0.29, 0.30, 0.31\}$.

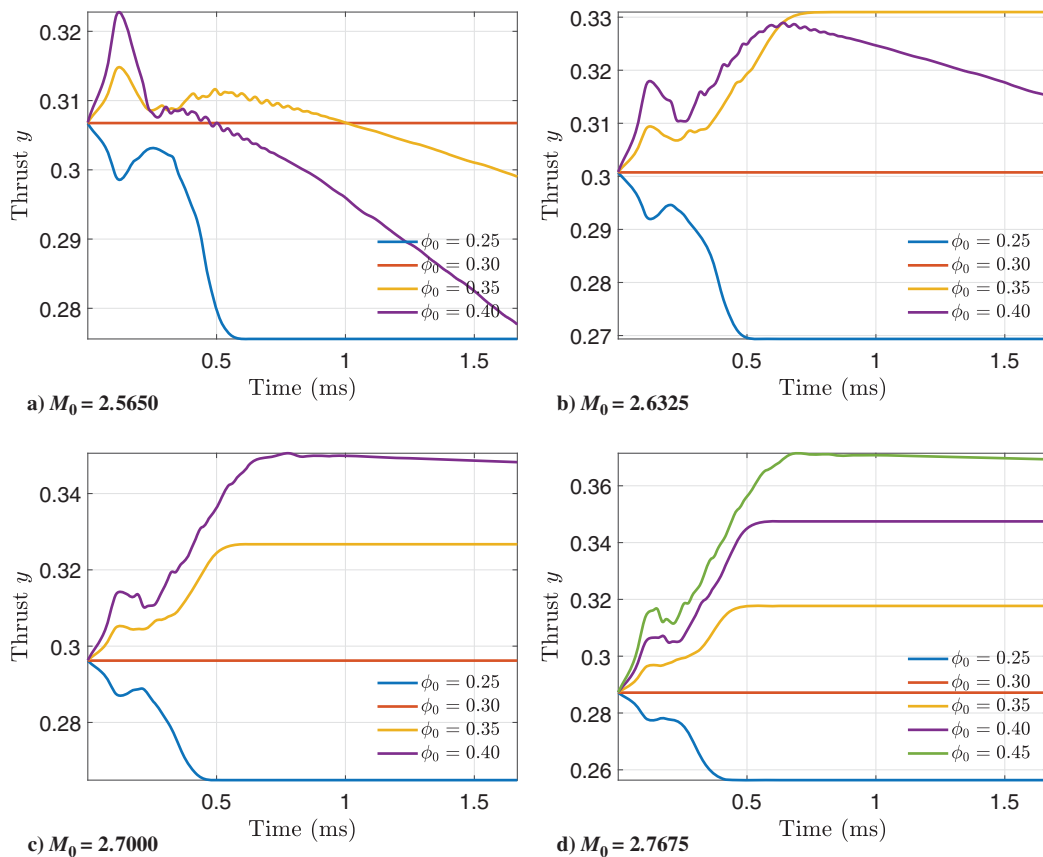


Fig. 4 Open-loop step response of the scramjet at various inlet Mach numbers.

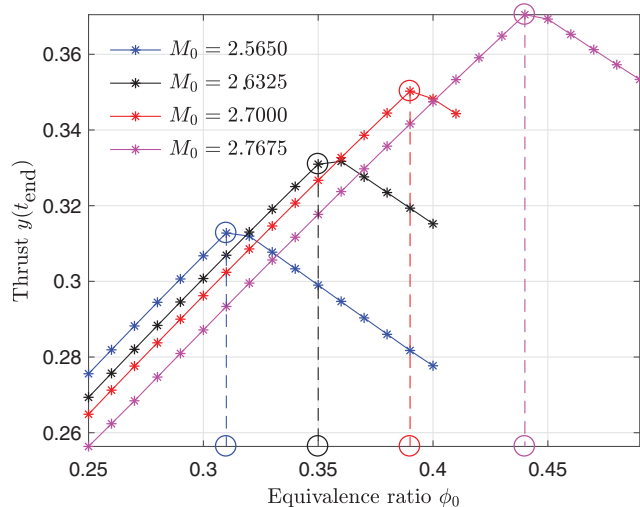


Fig. 5 Open-loop step response of the scramjet at various inlet Mach numbers and equivalence ratios.

If the flow were entirely supersonic, the thrust would rise monotonically and then decay. However, the presence of subsonic pockets introduces wave perturbations that propagate both upstream and downstream, giving rise to a more complex impulse response. Note that the impulse response δy changes qualitatively as ϕ_0 changes, thus indicating that the equivalence ratio has a nonlinear effect on the state of the scramjet. Figure 7b shows the impulse response of the scramjet for fixed $\phi_0 = 0.30$ and impulse magnitudes $\phi_\delta \in \{0.05, 0.10\}$.

In discrete-time linear systems, the elements of the impulse response form the Markov parameter sequence. Using these Markov parameters, the original linear system can be reconstructed by applying system identification techniques [20–23]. The impulse response is then used to construct a linearized model of the scramjet at

an equilibrium state. The local behavior of the linearized model can then be analyzed.

A finite impulse response (FIR) model structure is used to construct a linear approximation to the scramjet. An n th-order FIR model can be written as

$$\tilde{y}(k) = \sum_{i=0}^n a_i \tilde{\phi}(k-i) \quad (6)$$

where \tilde{y} is the thrust perturbation, $\tilde{\phi}$ is the equivalence-ratio perturbation, and a_i are the coefficients to be fitted using the impulse response of the scramjet. The transfer function from $\tilde{\phi}$ to \tilde{y} can be written as

$$G_{\text{FIR}}(\mathbf{q}) = \frac{a_1 \mathbf{q}^n + \cdots + a_n}{\mathbf{q}^n} \quad (7)$$

where \mathbf{q} is the forward-shift operator. Note that all poles of the discrete-time transfer function G_{FIR} are at zero, and thus G_{FIR} is asymptotically stable.

We use the impulse response obtained at the equivalence ratio $\phi_0 = 0.30$ and inlet Mach number $M_0 = 2.7$ with the impulse magnitude $\phi_\delta = 0.05$ to construct the FIR approximation. Thus, $\tilde{\phi}(0) = 0.05$, $\tilde{\phi}(k) = 0$ for all $k \geq 1$, and $\tilde{y}(k) = \delta y(k)$. The n th-order FIR model is constructed using the first n Markov parameters. Note that, if $\tilde{\phi}(k) = \phi_\delta \delta(k)$, where $\delta(\cdot)$ is the discrete-delta function, then $\tilde{y}(k) = \delta y(k)$. Consequently, $a_i = \tilde{y}(i)/\tilde{\phi}(0)$. Figure 8a shows the pole-zero map of the fitted FIR model of order 1031, which is the length of the impulse response sequence, and Fig. 8b shows a magnified view of the pole-zero map near the NMP zeros. Note that the approximate FIR model has three pairs of complex NMP zeros. From the pole-zero plot of the FIR model approximation of the scramjet, we conclude that the scramjet dynamics possess NMP behavior. Note that the goal is to ascertain the existence of NMP behavior of the system only and not to find an accurate model of the

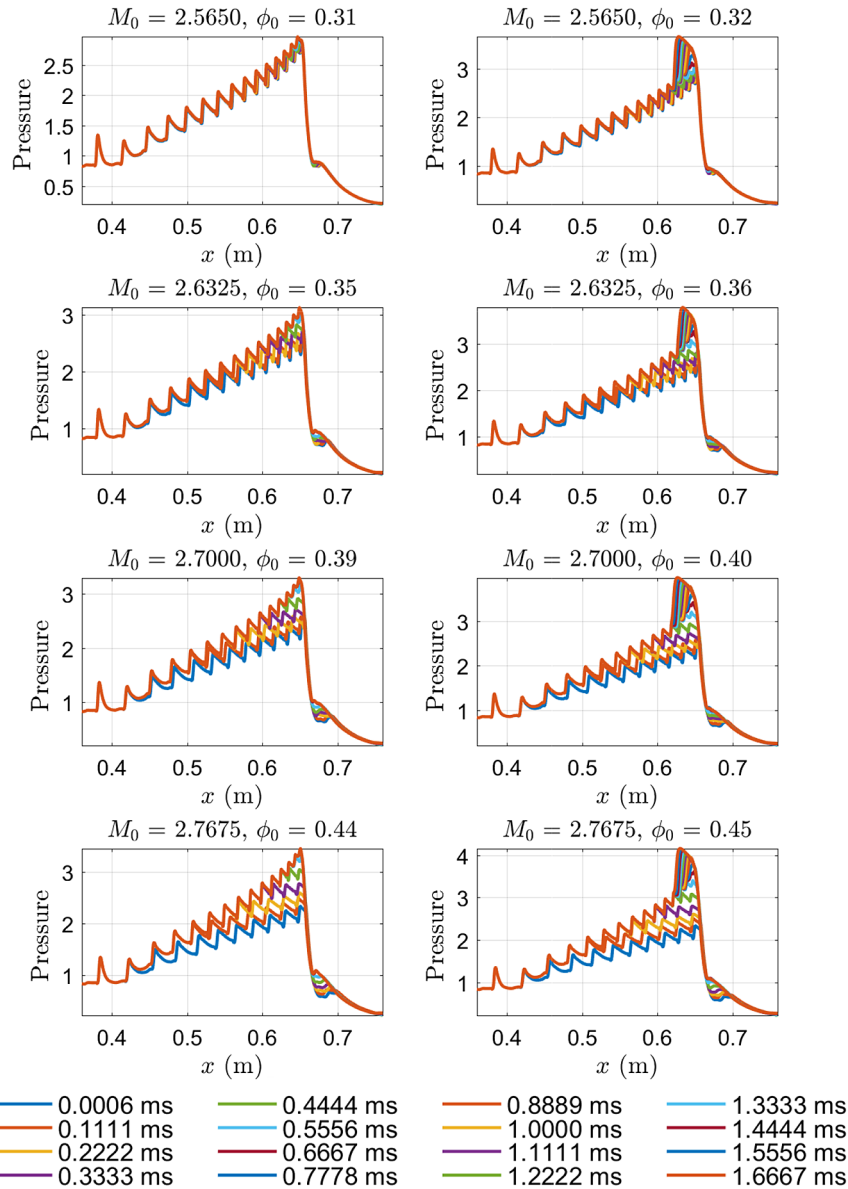


Fig. 6 Normalized static pressure along the lower wall of the scramjet at various inlet Mach numbers and equivalence ratios.

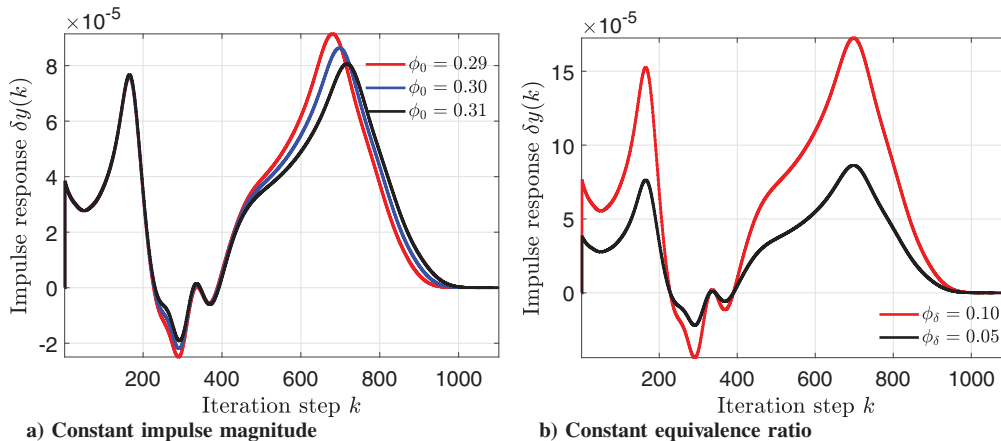


Fig. 7 Impulse response of the scramjet. The inlet Mach number satisfies $M_0 \equiv 2.7$ for all cases considered.

scramjet dynamics. In effect, the FIR model that exhibits NMP behavior is a highly simplified reduced-order model of the scramjet required by RCAC.

IV. Adaptive Control Algorithm

In this section, we present the underlying principles and algorithmic details of RCAC. In RCAC, the controller coefficients

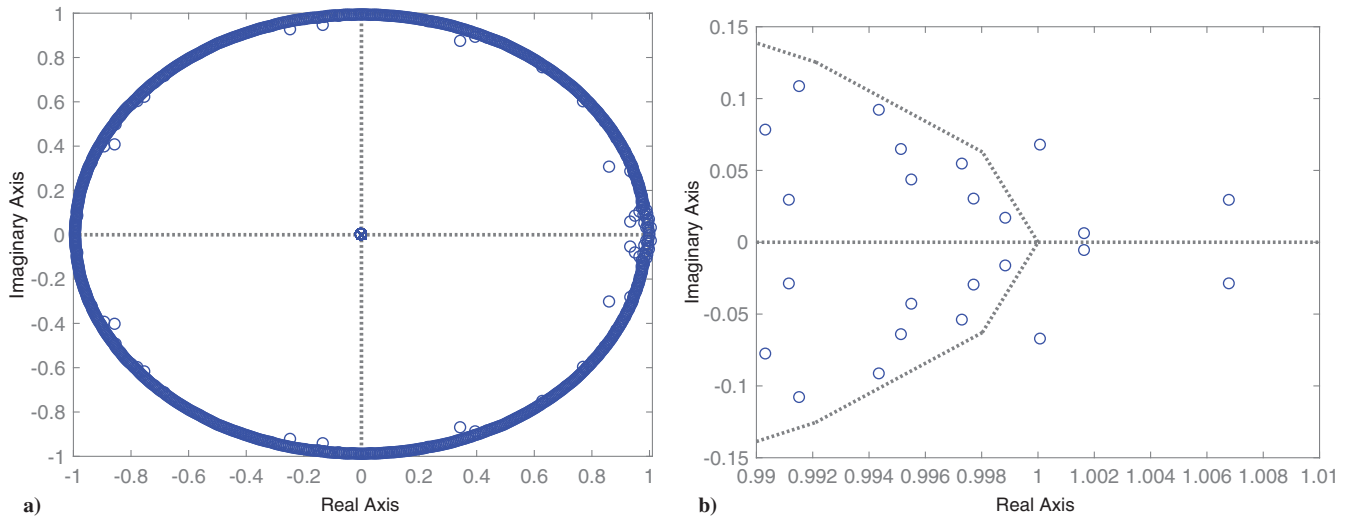


Fig. 8 Pole-zero map of the FIR transfer function constructed from the impulse response.

are updated by minimizing a retrospective cost function. The retrospective cost depends on input and output data as well as limited modeling information. A detailed description of the RCAC algorithm as well as the modeling information required for implementation are described in [9].

A. Plant Model

Consider a system modeled by the discrete-time dynamics

$$x(k+1) = f(x(k), u_c(k), w(k)) \quad (8)$$

$$y(k) = g(x(k), u_c(k), w(k)) \quad (9)$$

$$z(k) = h(x(k), u_c(k), w(k)) \quad (10)$$

where $x(k) \in \mathbb{R}^{l_x}$ is the state; $y(k) \in \mathbb{R}^{l_y}$ is the measurement; $u_c \in \mathbb{R}^{l_u}$ is the control signal; $w(k) \in \mathbb{R}^{l_w}$ is the exogenous signal; and $z(k) \in \mathbb{R}^{l_z}$ is the performance variable. The goal is to develop an adaptive output-feedback controller that minimizes a function of z in the presence of the exogenous signal w with limited modeling information about Eqs. (8–10). The components of w can represent command signals to be followed, external disturbances to be rejected, or both.

B. Controller

Consider the linear time-varying output-feedback controller

$$u_c(k) = \sum_{i=1}^{n_c} M_i(k) u_c(k-i) + \sum_{i=1}^{n_c} N_i(k) \xi(k-i) \quad (11)$$

where $M_i(k) \in \mathbb{R}^{l_u \times l_u}$, $N_i(k) \in \mathbb{R}^{l_u \times l_z}$ are the controller coefficient matrices, and the components of the vector $\xi(k) \in \mathbb{R}^{l_z}$ consist of components of the output y , the performance variable z , and the exogenous signal w . At each time step, RCAC updates the coefficients $M_i(k)$ and $N_i(k)$ to minimize a function of the performance variable z . We rewrite Eq. (11) as

$$u_c(k) = \Phi(k) \theta(k) \quad (12)$$

where the regressor matrix $\Phi(k)$ is defined by

$$\Phi(k) \triangleq I_{l_u} \otimes \begin{bmatrix} u_c(k-1)^T & \dots & u_c(k-n_c)^T & \xi(k-1)^T & \dots & \xi(k-n_c)^T \end{bmatrix} \in \mathbb{R}^{l_u \times l_\theta} \quad (13)$$

$$\theta(k) \triangleq \text{vec} \begin{bmatrix} M_1(k) & \dots & M_{n_c}(k) & N_1(k) & \dots & N_{n_c}(k) \end{bmatrix} \in \mathbb{R}^{l_\theta} \quad (14)$$

where $l_\theta \triangleq l_u n_c (l_u + l_z)$, I_{l_u} is the $l_u \times l_u$ identity matrix, \otimes is the Kronecker product, and “vec” is the column-stacking operator [24].

C. Retrospective Performance Variable

The retrospective performance variable is defined by

$$\hat{z}(k) \triangleq z(k) + G_f(\mathbf{q})(\Phi(k) \hat{\theta} - u_c(k)) = z(k) + \Phi_f(k) \hat{\theta} - u_f(k) \quad (15)$$

where \mathbf{q} is the forward shift operator in the time domain:

$$G_f(\mathbf{q}) = \sum_{i=1}^{n_f} \frac{N_i}{\mathbf{q}^i}, \quad N_i \in \mathbb{R}^{l_z \times l_u} \quad (16)$$

$$\Phi_f(k) \triangleq G_f(\mathbf{q}) \Phi(k) = \sum_{i=1}^{n_f} N_i \Phi(k-i) \quad (17)$$

$$u_f(k) \triangleq G_f(\mathbf{q}) u_c(k) = \sum_{i=1}^{n_f} N_i u_c(k-i) \quad (18)$$

Note that $\hat{\theta}$ contains the controller coefficients to be optimized. The filter G_f is the key component needed to implement RCAC. The analysis of the ideal filter G_f^* is presented in [8], and multiple interpretations of G_f are discussed in [9]. The filter G_f requires knowledge of the linearized dynamics relating u to z , namely, the relative degree, the sign of the leading term of the impulse response, and approximate knowledge of the real NMP zeros.

D. Retrospective Cost Function

In terms of the retrospective performance variable $\hat{z}(k)$, the retrospective cost function is defined by

$$J(k, \hat{\theta}) \triangleq \sum_{i=1}^k \lambda^{k-i} \hat{z}^T(i) R_z \hat{z}(i) + \hat{\theta}^T R_\theta \hat{\theta} \quad (19)$$

where the performance weighting R_z and the controller coefficient weighting R_θ are positive-definite matrices, and $\lambda \in (0, 1]$ is the forgetting factor. Setting $\lambda < 1$ emphasizes the latest measurements, which facilitates the response to changing conditions.

Algorithm 1 RCAC algorithm

Input	$u_c(k-1), y(k-1), z(k-1)$.
Output	$\theta(k), u_c(k)$.
Algorithm	1) Construct $u_c(k)$ using Eq. (13). 2) Compute $\Phi_f(k+1)$ and $u_f(k)$ using Eqs. (17) and (18). 3) Update $\theta(k)$ and $P(k)$ using Eqs. (20) and (21). 4) Compute $u_c(k)$ using Eq. (23).

Proposition: Let $P(0) = R_\theta^{-1}$ and $\theta(0) = 0$. Then, for all $k \geq 1$, the retrospective cost function [Eq. (19)] has a unique global minimizer $\theta(k)$, which is given by

$$\theta(k) = \theta(k-1) - P(k)\Phi_f^T(k)(\Phi_f(k)\theta(k-1) + z(k) - u_f(k)) \quad (20)$$

$$P(k) = \frac{1}{\lambda}P(k-1) - \frac{1}{\lambda}P(k-1)\Phi_f^T(k)\Gamma(k)\Phi_f(k)P(k-1) \quad (21)$$

where

$$\Gamma(k) \triangleq (\lambda I_{l_z} + \Phi_f(k)P(k-1)\Phi_f^T(k))^{-1} \quad (22)$$

The corresponding optimal control at time step k is given by

$$u_c(k) = \Phi(k)\theta(k) \quad (23)$$

At time step $k-1$, input $u_c(k-1)$ is applied to the system, the output $y(k-1)$ is measured, and the performance variable $z(k-1)$ is computed. Therefore, $u_c(k-1)$, $y(k-1)$, and $z(k-1)$ are known at step $k-1$. These numerical values are used by RCAC to produce $u_c(k)$, which is applied at the k th step. Algorithm 1 summarizes the RCAC algorithm used to compute $u_c(k)$.

V. Adaptive Control of the Two-Dimensional Scramjet

RCAC is now used to follow a thrust command at a constant inlet Mach number and maintain constant thrust in the presence of unknown changes in the inlet Mach number. RCAC is also applied to the problem of preventing the scramjet from unstating. Note that the scramjet can unstart due to either a perturbation in the inlet flow conditions or an increase in the commanded thrust.

RCAC is a discrete-time direct adaptive control algorithm that operates at a constant sample rate. In this paper, the time step used by RCAC is $T_c = 1.25 \times 10^{-2}$ ms. Note that $T_c = 25T_s$, that is, the scramjet state is updated 25 times for every update of the equivalence ratio by RCAC. In the following numerical simulations, the continuous-time variable t and the discrete time variable k are related by $t = kT_c$.

We define the performance variable

$$z(k) \triangleq y(k) - r(k) \quad (24)$$

where $y(k)$ is the thrust generated by the scramjet, and $r(k)$ is the commanded thrust. The equivalence ratio is given by $\phi(k) = \phi_0 + \bar{u}_c(k)$, where $\bar{u}_c(k)$ is the saturated value of $u_c(k)$. The saturation function enforces the nonnegativity of ϕ and is sufficiently restrictive to prevent the controller from inducing unstart. In Sec. V.B, the upper limit on the equivalence ratio will be increased

to study unstart suppression. Figure 9 shows the architecture used by RCAC and all relevant variables.

We use a strictly proper feedforward and feedback controller architecture of order n_c , which can be represented in time-series form as

$$u_c(k) = \sum_{i=1}^{n_c} M_i(k)u_c(k-i) + \sum_{i=1}^{n_c} N_i(k) \begin{bmatrix} z(k-i) \\ r(k-i) \end{bmatrix} = \Phi(k)\theta(k) \quad (25)$$

where $\theta(k) \in \mathbb{R}^{3n_c}$ contains the coefficients $M_i(k)$ and $N_i(k)$ adapted by RCAC, and $\Phi(k) \in \mathbb{R}^{1 \times 3n_c}$ is the regressor vector containing previous inputs and measurements.

In the following numerical examples, we simulate the scramjet dynamics from the equilibrium state achieved with a constant equivalence ratio $\phi_0 \equiv 0.30$ at a constant inlet Mach number $M_0 \equiv 2.7$.

A. Command Following and Disturbance Rejection

In this section, we present the closed-loop response of the scramjet to a constant step command, a changing step command, and a ramp command. To focus on the normal operation of the scramjet, we assume that the commanded thrust is less than the critical thrust at the given operating condition.

1. Step Command

The scramjet is commanded to generate a constant thrust given by $r(k) = 0.26$ for all $k \geq 1$ at a constant inlet Mach number $M_0 \equiv 2.7$. At $k = 1$, RCAC is switched on. The filter is set to be $G_f(\mathbf{q}) = 0.1/\mathbf{q}$, and the controller order is $n_c = 2$. The retrospective cost weightings are $R_z = 1$, $R_\theta = 0.1I_{l_\theta}$, and $\lambda = 1$. The closed-loop response is shown in Fig. 10. Figure 10a shows the thrust y generated by the scramjet; Fig. 10b shows the equivalence ratio ϕ computed by RCAC; Fig. 10c shows the performance variable z ; Fig. 10d shows the controller coefficients θ computed by RCAC; Fig. 10e shows the normalized static pressure along the lower wall; Fig. 10f shows the Mach number along the lower wall; Fig. 10g shows the normalized static pressure along the lower wall for several time steps; and Fig. 10h shows the Mach number along the lower wall for several time steps.

Next, we investigate the effect of the filter G_f on the closed-loop response of the scramjet. The controller order is $n_c = 2$, and the retrospective cost weightings are $R_z = 1$, $R_\theta = 0.1I_{l_\theta}$, and $\lambda = 1$. For several choices of G_f , the closed-loop response is shown in Fig. 11.

2. Changing Step Command

The scramjet is commanded to follow a sequence of constant thrust commands given by $r(k) = 0.27$ for $k \leq 333$, $r(k) = 0.32$ for $333 < k \leq 666$, and $r(k) = 0.28$ for $k > 666$ at the constant inlet Mach number $M_0 \equiv 2.7$. At $k = 1$, RCAC is switched on. The filter is set to be $G_f(\mathbf{q}) = 0.1/\mathbf{q}$, and the controller order is $n_c = 2$. The retrospective cost weightings are $R_z = 1$, $R_\theta = 0.1I_{l_\theta}$, and $\lambda = 1$. The closed-loop response is shown in Fig. 12.

3. Ramp Command

The scramjet is commanded to follow a ramp thrust command given by $r(k) = 0.29 - 1.5 \times 10^{-5}k$ for $k \geq 1$ at a constant inlet

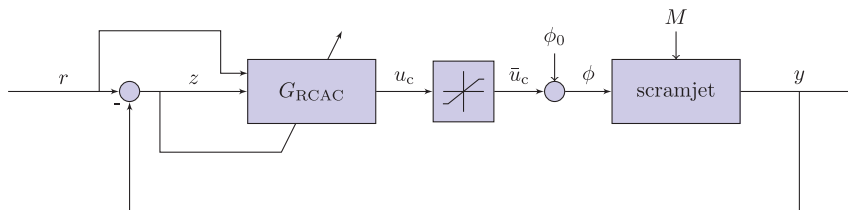


Fig. 9 Control system architecture. The controller G_{RCAC} is updated by RCAC. The controller structure used for this application is given by Eq. (25).

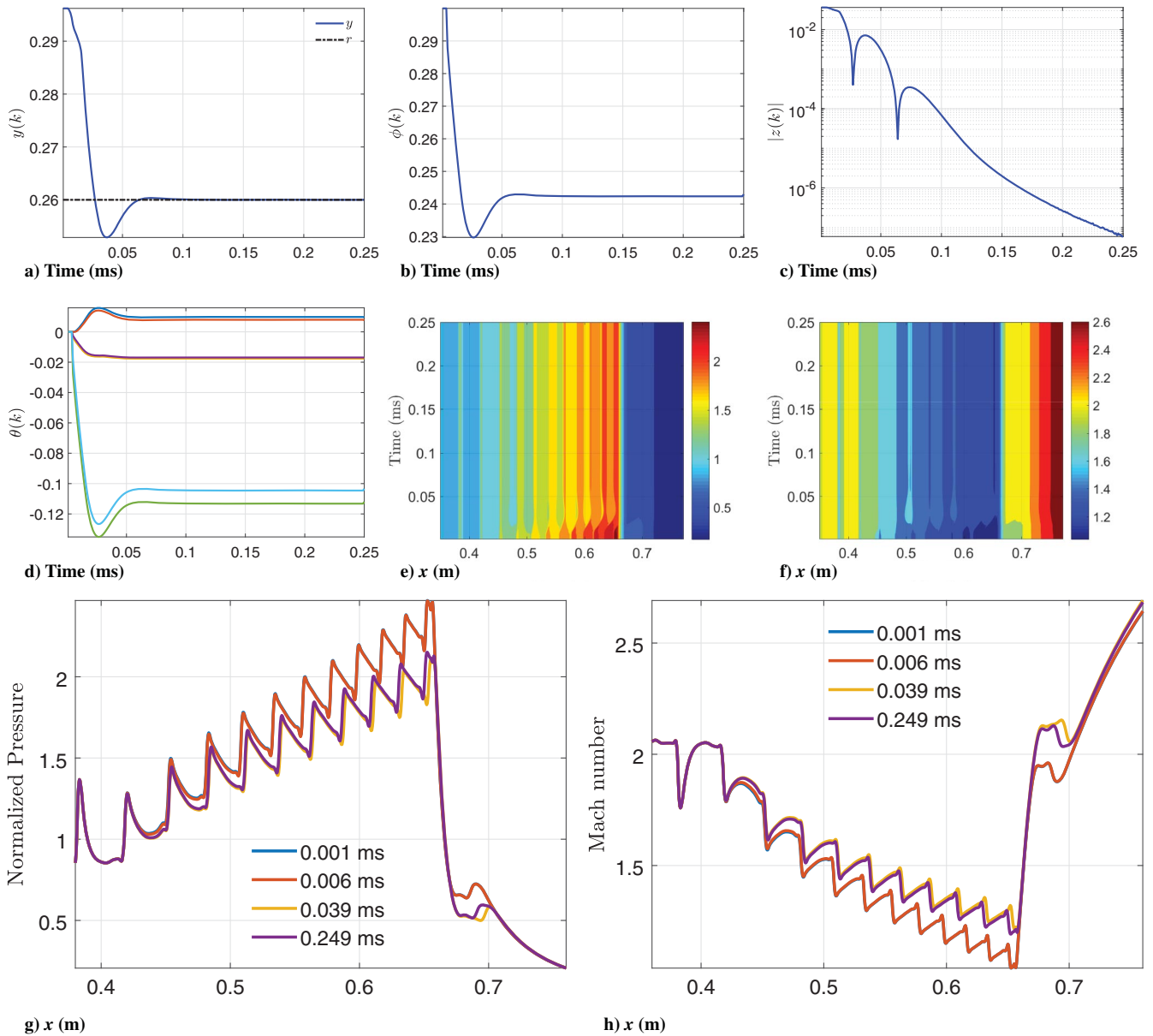


Fig. 10 Closed-loop response of the scramjet to a step command.

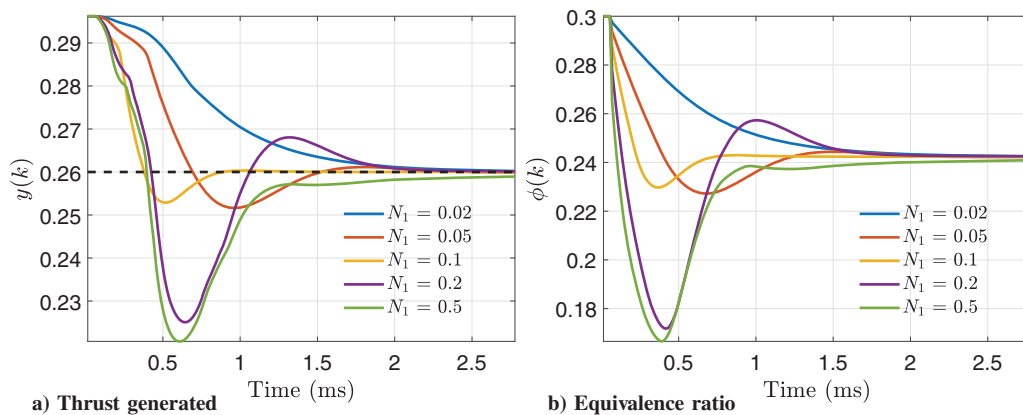


Fig. 11 Closed-loop response of the scramjet to a step command for various choices of $G_f(q) = N_1/q$. The step command is indicated by the dashed black line.

Mach number $M_0 \equiv 2.7$. At $k = 1$, RCAC is switched on. The filter is set to be $G_f(q) = 0.1/q$, and the controller order is $n_c = 2$. The retrospective cost weightings are $R_z = 1$, $R_\theta = 0.1I_\theta$, and $\lambda = 1$. The closed-loop response is shown in Fig. 13.

4. Disturbance Rejection

The scramjet is commanded to generate a constant thrust given by $r(k) = 0.28$ for all $k \geq 1$ when the inlet Mach number has an unknown change. The inlet Mach number $M(k) = 2.7$ for $k \leq 300$,

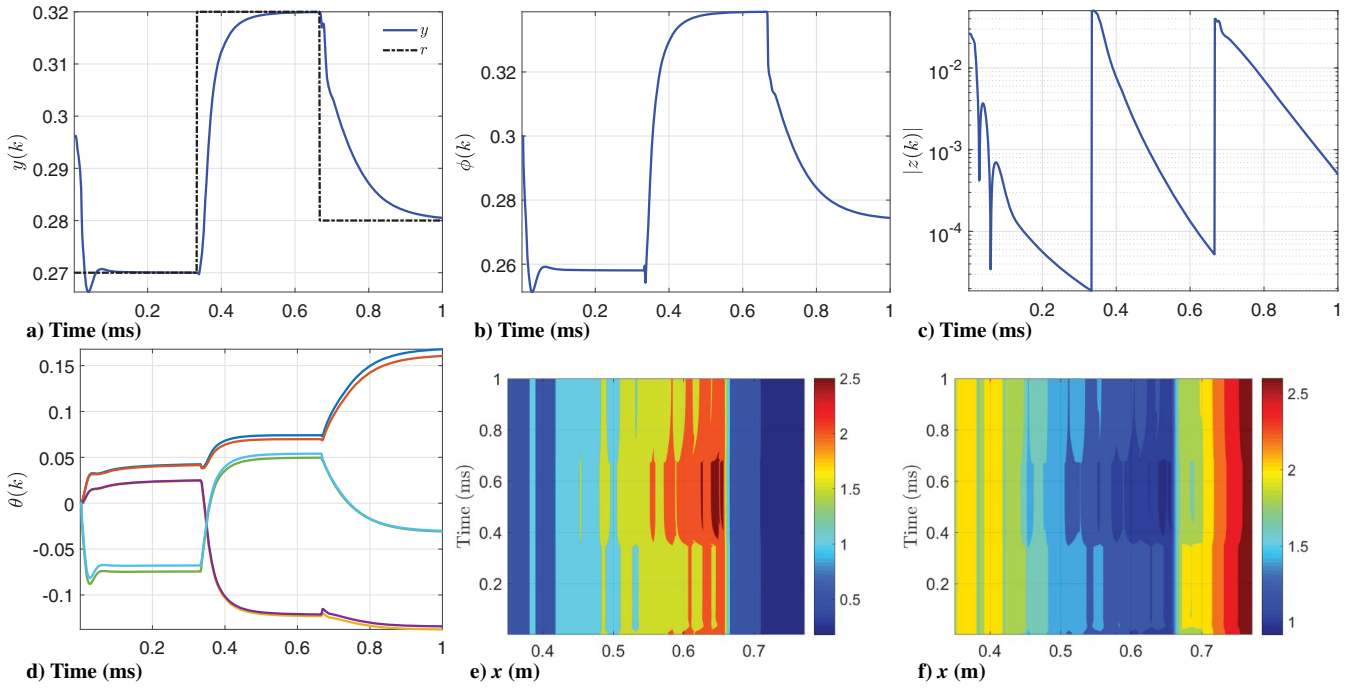


Fig. 12 Closed-loop response of the scramjet to a sequence of step commands.

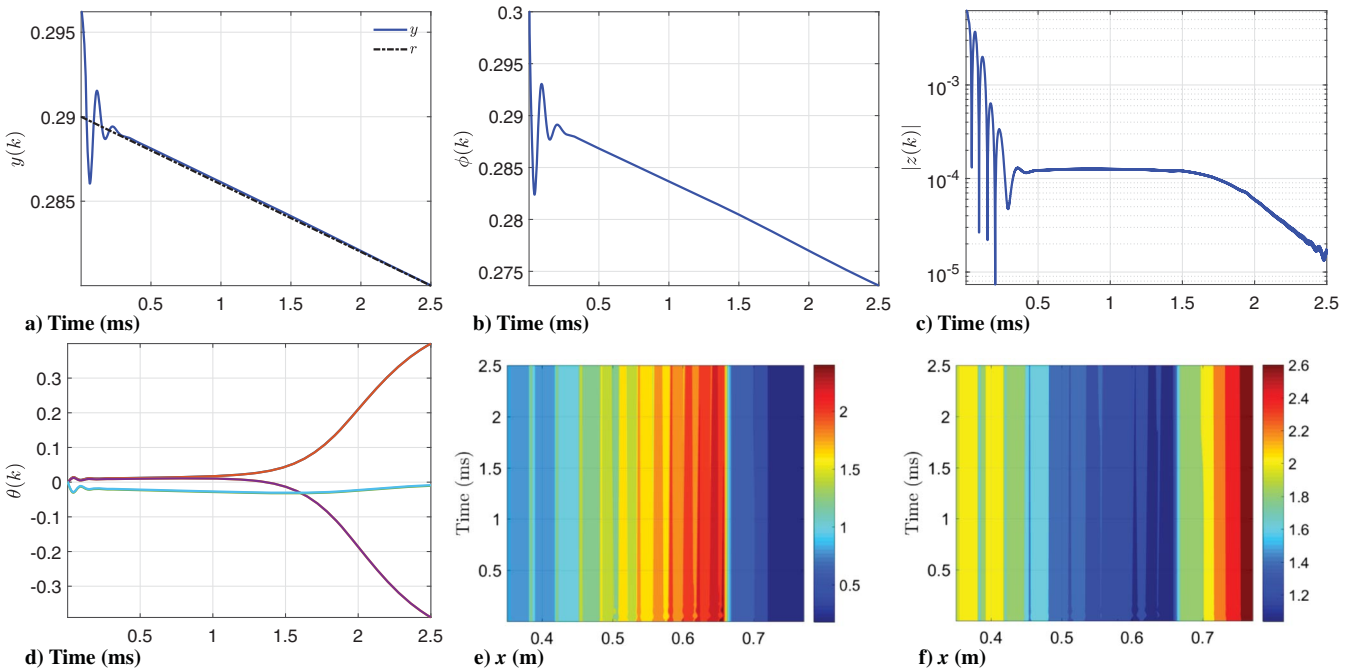


Fig. 13 Closed-loop response of the scramjet to a ramp command.

$M(k) = 2.7(1 + (0.1/50)(k - 300))$ for $300 < k \leq 350$, and $M(k) = 2.97$ for $k > 350$. At $k = 1$, RCAC is switched on. The filter is set to be $G_f(q) = 0.1/q$, and the controller order is $n_c = 2$. The retrospective cost weightings are $R_z = 1$, $R_\theta = 0.1I_{l_\theta}$, and $\lambda = 0.995$. The closed-loop response is shown in Fig. 14. Note that, as the inlet Mach number increases, the equivalence ratio required to maintain same thrust also increases, which is a characteristic of the physics of the problem. However, RCAC uses no knowledge of the dynamical relationship between the inlet Mach number and the generated thrust to compute the required equivalence ratio.

B. Unstart Control

In this section, we consider the problem of preventing the scramjet from unstating. Specifically, we consider the problem of

preventing a normal shock from traveling upstream as well as maintaining the thrust near the command when the commanded thrust is greater than the critical thrust. As mentioned earlier, the scramjet can unstart due to either excessive heat addition or a perturbation in the inlet flow conditions. We consider the problem of preventing unstart that occurs when the commanded thrust is above the critical thrust at the operating inlet Mach number. In such a case, the scramjet unstarts due to excessive heat addition. Figures 4–6 show that, at the inlet Mach number $M_0 = 2.7$, the scramjet unstarts when $\phi_0 = 0.40$. Numerical simulations and experimental measurements at DLR suggest that the scramjet generates critical thrust at $\phi = 0.39$, that is, when $\phi(k) \equiv \phi_0 = 0.39$, the scramjet is able to attain a steady state at a constant inlet Mach number $M(k) \equiv M_0 = 2.7$.

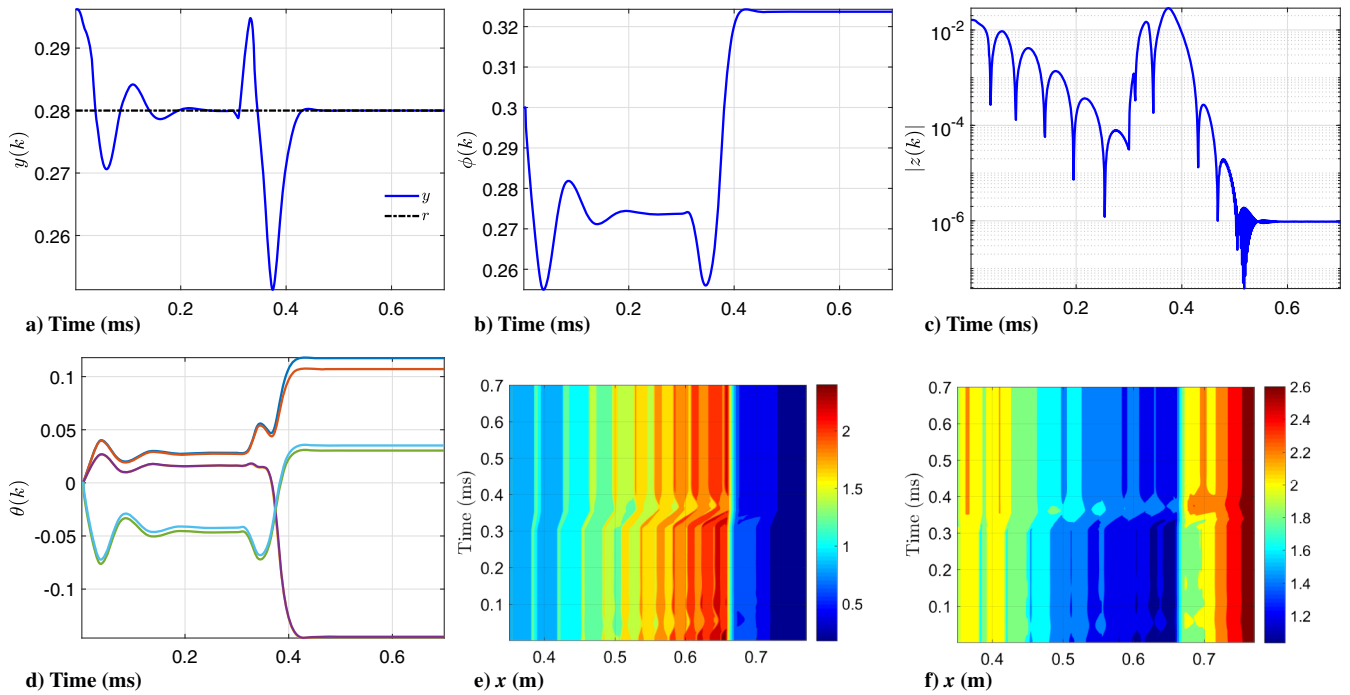


Fig. 14 Closed-loop response of the scramjet subjected to a step change in the inlet Mach number.

Once the scramjet unstarts, the qualitative relationship between the equivalence ratio ϕ and the generated thrust y changes. When the scramjet is operating sufficiently away from unstart limits, increasing the equivalence ratio ϕ increases the generated thrust. However, when the scramjet is unstarting, the state of the scramjet is unsteady, and increasing the equivalence ratio ϕ decreases the generated thrust y .

As mentioned earlier, the filter G_f used by RCAC requires the correct sign of the leading Markov parameter. The condition approximately translates to the qualitative relationship between the input and the output of the single-input/single-output system. If increasing the input increases the steady-state output value, the leading coefficient of the filter G_f should be positive, and vice versa.

Therefore, when the scramjet unstarts, the leading coefficient of the filter G_f must change sign from positive to negative. However, identifying unstart from the thrust measurements is challenging because it is difficult to distinguish between benign scramjet dynamics transients and thrust loss due to a normal shock advancing upstream.

A functional is defined in [13] based on the pressure profile on the upper wall of the combustor. It was observed in [13] that values of the functional above a critical value indicate the presence of a normal shock wave in the combustor, which indicates unstart. In the present paper, we use a single pressure measurement. We stress, however, that the method used to identify unstart is immaterial as far as RCAC is concerned.

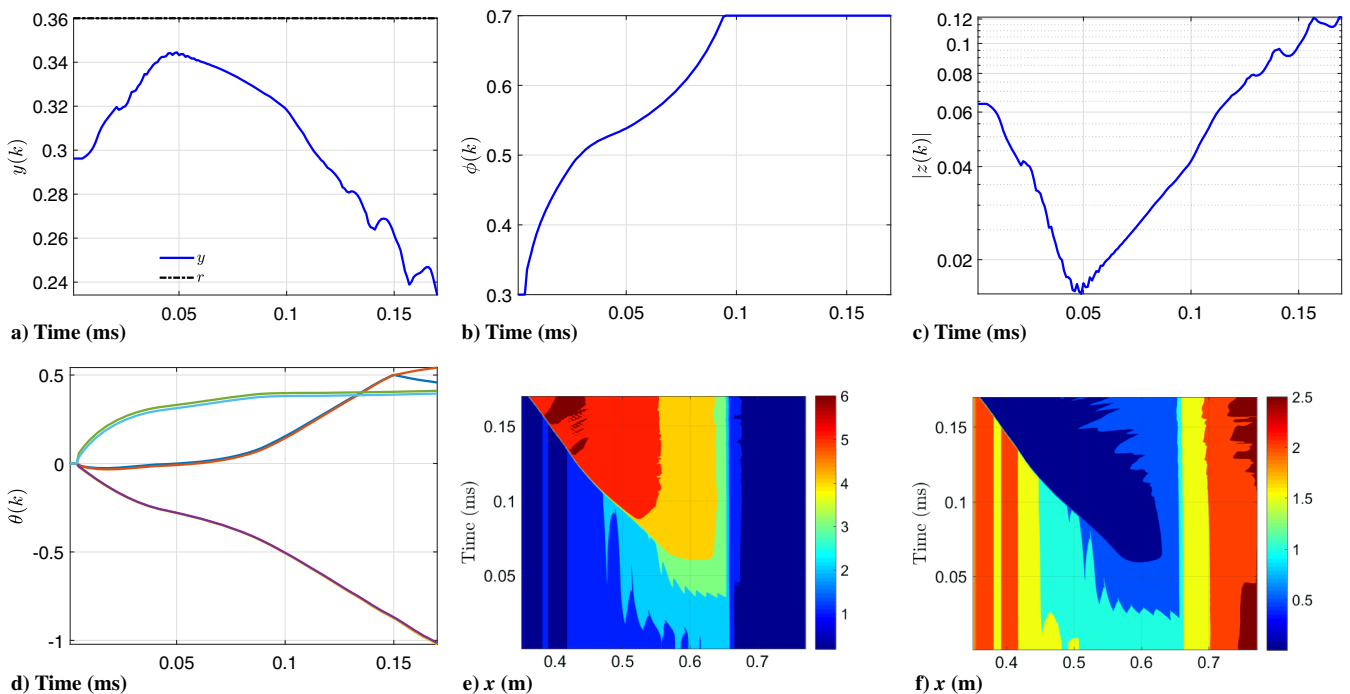


Fig. 15 Closed-loop response of the scramjet commanded to follow a thrust command greater than the critical thrust at the given operating condition without using the modified performance variable.

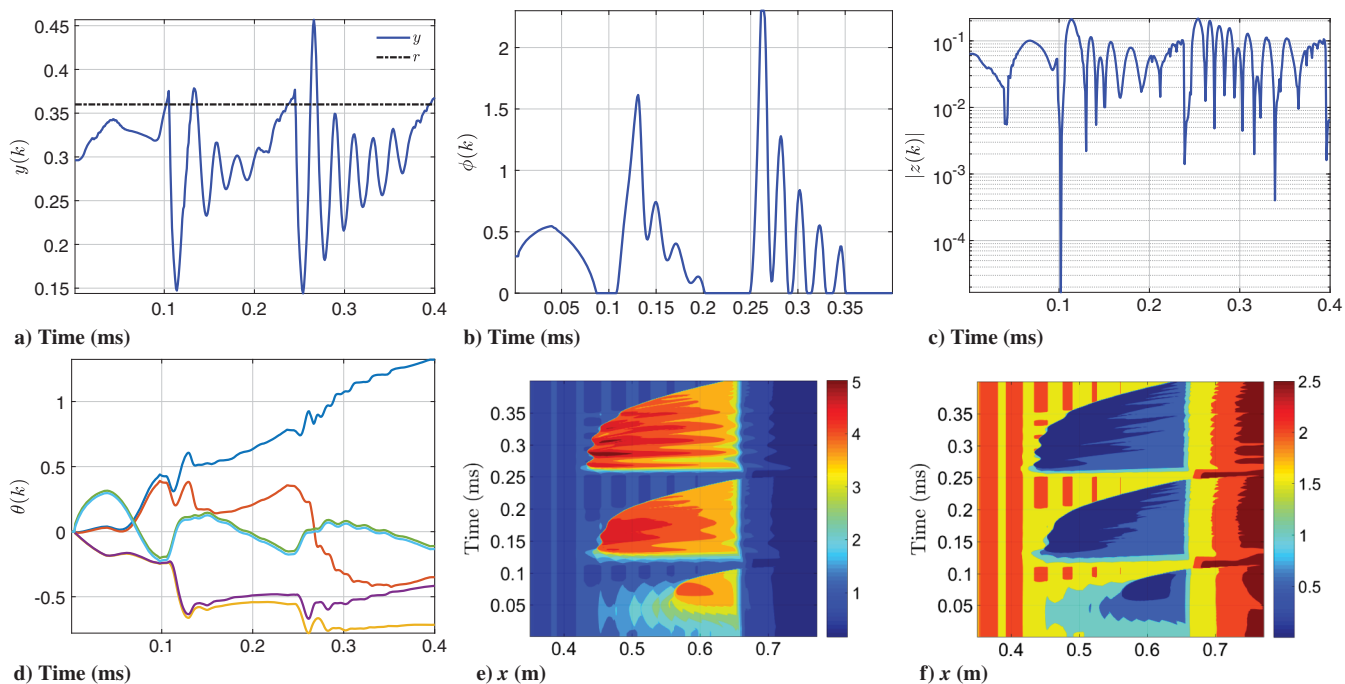


Fig. 16 Closed-loop response of the scramjet commanded to follow a thrust command greater than the critical thrust at the given operating condition using the modified performance variable [Eq. (26)].

In Fig. 6, it was shown that the normalized static pressure at $x = 0.625$ m is below 3.1 during normal operation and above 3.1 during unstart. The performance variable z originally defined by Eq. (24) is thus modified as

$$z(k) \triangleq y(k) - r(k) + R_{\text{un}} \max\{P_{0.625}(k) - 3.1, 0\} \quad (26)$$

where R_{un} is a positive weighting that affects the response of the controller to unstart, and $P_{0.625}(k)$ is the normalized static pressure measurement at $x = 0.625$ m at time step k . By minimizing the norm of the performance variable z , RCAC adjusts the equivalence ratio $\phi(k)$ to maintain the normalized static pressure at $x = 0.625$ m below 3.1 and hence prevents the normal shock from travelling upstream.

First, we present the closed-loop response of the scramjet without the modified performance variable, that is, without unstart control. Note that this is equivalent to setting $R_{\text{un}} = 0$ in Eq. (26). The scramjet is commanded to generate a constant thrust given by $r(k) = 0.36$ for all $k \geq 1$ at a constant inlet Mach number $M_0 \equiv 2.7$, which is above the critical thrust at $M_0 = 2.7$. The filter is set to be $G_f(\mathbf{q}) = 0.1/\mathbf{q}$, and the controller order is $n_c = 2$. The retrospective cost weightings are $R_z = 1$, $R_\theta = 0.1I_{l_\theta}$, and $\lambda = 1$. The equivalence ratio $\phi(k) = 0.30 + \bar{u}_c(k)$, where $\bar{u}_c(k)$ is the saturated value of $u_c(k)$. In contrast to Sec. V.A, where the upper saturation limit was chosen to prevent unstart, the upper bound of the saturation is now increased to allow the controller to induce unstart. Figure 15 shows the closed-loop response of the scramjet without unstart control. Note that the normal shock travels upstream, and flow becomes completely subsonic in the isolator section.

Next, we present the closed-loop response of the scramjet with unstart control. The scramjet is commanded to generate a constant thrust given by $r(k) = 0.36$ for all $k \geq 1$ at a constant inlet Mach number $M_0 \equiv 2.7$, which is above the critical thrust at $M_0 = 2.7$. The filter is set to be $G_f(\mathbf{q}) = 0.1/\mathbf{q}$, and the controller order is $n_c = 2$. The retrospective cost weightings are $R_z = 1$, $R_\theta = 0.1I_{l_\theta}$, $\lambda = 1$, and $R_{\text{un}} = 0.15$. Figure 16 shows the closed-loop response of the scramjet with unstart control. With the modified performance variable, RCAC adjusts the equivalence ratio ϕ so that the normal shock does not reach the inlet. Note that it is physically impossible for the scramjet to generate the commanded thrust in steady state. Consequently, because

unstart prevention is prioritized over command following, the scramjet reaches a limit-cycle-like condition.

VI. Conclusions

This paper used retrospective cost adaptive control (RCAC) to control the thrust generated by a scramjet. RCAC uses data to adjust the controller coefficients and thus requires minimal modeling information concerning the relationship between the control input and the performance variable. This modeling information is used to construct the filter G_f , which is used to update the controller coefficients. The filter G_f can be constructed by analyzing the impulse response of the scramjet. Specifically, in terms of a linearized model, RCAC uses the sign of the first nonzero element of the impulse response, the relative degree, and real nonminimum-phase (NMP) zeros to construct G_f .

The open-loop step response was used to establish the operational envelope of the scramjet in terms of the inlet Mach number and the equivalence ratio. Specifically, critical thrust, defined as the maximum steady-state thrust that the scramjet can generate at a constant inlet Mach number, was computed for various inlet conditions. The open-loop impulse response, from equivalence ratio to the generated thrust, was used to construct the filter G_f .

RCAC was applied to command following and disturbance rejection. Specifically, a constant step command, a sequence of step commands, and ramp commands at a constant inlet Mach number were considered. In addition, maintaining the commanded thrust in the presence of an uncertain step change in the inlet Mach number was considered. Finally, by modifying the performance variable, RCAC was used to prevent the scramjet from unstating.

As the scramjet unstarts, the flowfield breaks down in a fraction of millisecond. To prevent the scramjet from unstating, the control system must react at the time scale at which unstart occurs. This is a fundamental challenge emanating from the physics of the problem. It was shown that, with the modified performance variable and assuming the availability of a high-bandwidth actuator, RCAC is able to prevent the scramjet from unstating.

The required controller order depends on a combination of the command, disturbance, and dynamics. Numerical testing was used to determine an adequate controller order. For the relevant commands

and disturbance, a second-order multi-input/single-output controller was found to be effective.

Although promising results for step-command following, step-disturbance rejection, and unstart avoidance are presented, robustness to input and measurement noise, the effect of the initial state of the scramjet, alternative controller structures, and the robustness to the choice of the filter G_f remain to be explored.

Acknowledgments

This research was supported by the National Science Foundation (NSF) Civil, Mechanical and Manufacturing Innovation grant 1634709, NSF Chemical, Bioengineering, Environmental, and Transport Systems grant 1507928, and U.S. Air Force Office of Scientific Research Dynamic Data-Driven Application Systems grant FA9550-16-1-0071.

References

- [1] Smart, M. K., Hass, N. E., and Paull, A., "Flight Data Analysis of the Hyshot 2 Scramjet Flight Experiment," *AIAA Journal*, Vol. 44, No. 10, 2006, pp. 2366–2375.
doi:10.2514/1.20661
- [2] Brocanelli, M., Gunbatar, Y., Serrani, A., and Bolender, M. A., "Robust Control for Unstart Recovery in Hypersonic Vehicles," *AIAA Guidance, Navigation, and Control Conference*, AIAA Paper 2012-4698, Aug. 2012.
doi:10.2514/6.2012-4698
- [3] Hutzler, J. R., "Scramjet Isolator Modeling and Control," ProQuest Dissertations Publ., U.S. Air Force Inst. of Technology Rept. AFIT/DS/ENY/11-19, Wright-Patterson AFB, OH, 2011.
- [4] Dalle, D. J., Driscoll, J. F., and Torrez, S. M., "Ascent Trajectories of Hypersonic Aircraft: Operability Limits Due to Engine Unstart," *Journal of Aircraft*, Vol. 52, No. 4, 2015, pp. 1345–1354.
doi:10.2514/1.C032801
- [5] West, N., Papanicolaou, G., Glynn, P., and Iaccarino, G., "A Numerical Study of Filtering and Control for Scramjet Engine Flow," *20th AIAA Computational Fluid Dynamics Conference*, AIAA Paper 2011-3848, June 2011.
doi:10.2514/6.2011-3848
- [6] Goel, A., Xie, A., Duraisamy, K., and Bernstein, D. S., "Retrospective Cost Adaptive Thrust Control of a 1D Scramjet with Mach Number Disturbance," *Proceedings of the American Control Conference*, Inst. of Electrical and Electronics Engineers (IEEE), Chicago, IL, July 2015, pp. 5551–5556.
doi:10.1109/ACC.2015.7172208
- [7] Santillo, M. A., and Bernstein, D. S., "Adaptive Control Based on Retrospective Cost Optimization," *Journal of Guidance, Control, and Dynamics*, Vol. 33, No. 2, 2010, pp. 289–304.
doi:10.2514/1.46741
- [8] Hoagg, J. B., and Bernstein, D. S., "Retrospective Cost Model Reference Adaptive Control for Nonminimum-Phase Systems," *Journal of Guidance, Control, and Dynamics*, Vol. 35, No. 6, 2012, pp. 1767–1786.
doi:10.2514/1.57001
- [9] Rahman, Y., Xie, A., Hoagg, J. B., and Bernstein, D. S., "A Tutorial and Overview of Retrospective Cost Adaptive Control," *Proceedings of the American Control Conference*, Inst. of Electrical and Electronics Engineers (IEEE), Boston, MA, Aug. 2016, pp. 3386–3409.
doi:10.1109/ACC.2016.7525440
- [10] Rahman, Y., Xie, A., and Bernstein, D. S., "Retrospective Cost Adaptive Control: Pole Placement, Frequency Response, and Connections with LQG Control," *IEEE Control Systems Magazine*, Vol. 37, No. 5, Oct. 2017, pp. 28–69.
doi:10.1109/MCS.2017.2718825
- [11] Hoagg, J. B., and Bernstein, D. S., "Nonminimum-Phase Zeros: Much to Do About Nothing," *IEEE Control Systems Magazine*, Vol. 27, No. 3, June 2007, pp. 45–57.
doi:10.1109/MCS.2007.365003
- [12] Schramm, J. M., Karl, S., Hannemann, K., and Steelant, J., "Ground Testing of the Hyshot II Scramjet Configuration in HEG," *15th AIAA International Space Planes and Hypersonic Systems and Technologies Conference*, AIAA Paper 2008-2547, April–May 2008.
doi:10.2514/6.2008-2547
- [13] Wang, Q., Duraisamy, K., Alonso, J. J., and Iaccarino, G., "Risk Assessment of Scramjet Unstart Using Adjoint-Based Sampling Methods," *AIAA Journal*, Vol. 50, No. 3, 2012, pp. 581–592.
doi:10.2514/1.J051264
- [14] Doolan, C., and Boyce, R., "A Quasi-One-Dimensional Mixing and Combustion Code for Trajectory Optimisation and Design Studies," *15th AIAA International Space Planes and Hypersonic Systems and Technologies Conference*, AIAA Paper 2008-2603, April–May 2008.
doi:10.2514/6.2008-2603
- [15] Pecnik, R., Terrapon, V. E., Ham, F., Iaccarino, G., and Pitsch, H., "Reynolds-Averaged Navier–Stokes Simulations of the Hyshot II Scramjet," *AIAA Journal*, Vol. 50, No. 8, 2012, pp. 1717–1732.
doi:10.2514/1.J051473
- [16] Duraisamy, K., and Alonso, J., "Adjoint Based Techniques for Uncertainty Quantification in Turbulent Flows with Combustion," *42nd AIAA Fluid Dynamics Conference and Exhibit*, AIAA Paper 2012-2711, June 2012.
doi:10.2514/6.2012-2711
- [17] Laurence, S. J., Schramm, J. M., Karl, S., and Hannemann, K., "An Experimental Investigation of Steady and Unsteady Combustion Phenomena in the HyShot II Combustor," *17th AIAA International Space Planes and Hypersonic Systems and Technologies Conference*, AIAA Paper 2011-2310, April 2011.
doi:10.2514/6.2011-2310
- [18] Sato, T., and Kaji, S., "Study on Steady and Unsteady Unstart Phenomena Due to Compound Choking and/or Fluctuations in Combustor of Scramjet Engines," *4th Symposium on Multidisciplinary Analysis and Optimization*, AIAA Paper 1992-5102, 1992.
doi:10.2514/6.1992-5102
- [19] Buchmann, O. A., "Thermal–Structural Design Study of an Airframe-Integrated Scramjet: Summary Report," NASA CR 3141, 1979.
- [20] Ljung, L., *System Identification: Theory for the User*, 2nd ed., Prentice–Hall Information and System Sciences Series, Prentice–Hall, New Jersey, Jan. 1999, pp. 8–16.
- [21] Juang, J.-N., *Applied System Identification*, Prentice–Hall, Englewood Cliffs, NJ, 1993.
- [22] Soderstrom, T., and Stoica, P., *System Identification*, Prentice–Hall, London, UK, 1989, pp. 60–83.
- [23] Van Pelt, T., and Bernstein, D. S., "Least Squares Identification Using μ -Markov Parameterizations," *Proceedings of the 37th IEEE Conference on Decision and Control*, 1998, IEEE Publ., Piscataway, NJ, Dec. 1998, pp. 618–619.
doi:10.1109/CDC.1998.760748
- [24] Bernstein, D. S., *Matrix Mathematics: Theory, Fact, and Formulas*, 2nd ed., Princeton Univ. Press, Princeton, NJ, 2009, pp. 439–458.

C. W. Rowley
Associate Editor